



Distributed charge/discharge control of energy storages in a renewable-energy-based DC micro-grid

Navid Eghtedarpour, Ebrahim Farjah

School of Electrical and Computer Engineering, Shiraz University, Shiraz, Iran
 E-mail: farjah@shirazu.ac.ir; efarjah@yahoo.com

Abstract: This paper proposes a control strategy for the stable operation of the micro-grid during different operating modes while providing the DC voltage control and well quality DC-loads supply. The proposed method adapts the battery energy storage system (BESS) to employ the same control architecture for grid-connected mode as well as the islanded operation with no need for knowing the micro-grid operating mode or switching between the corresponding control architectures. Furthermore, the control system presents effective charging of the battery in the micro-grid. When the system is grid connected and during normal operation, AC grid converter balances active power to ensure a constant DC voltage while the battery has the option to store energy for necessary usage. In order to achieve the system operation under islanding conditions, a coordinated strategy for the BESS, RES and load management including load shedding and considering battery state-of-charge (SoC) and battery power limitation is proposed. Seamless transition of the battery converter between charging and discharging, and that of grid side converter between rectification and inversion are ensured for different grid operating modes by the proposed control method. **MATLAB/SIMULINK** simulations and experimental results are provided to validate the effectiveness of the proposed battery control system.

1 Introduction

Renewable-energy-based micro-grids have appeared to be a better way of exploiting renewable energy and reducing the environmental risks of fossil fuels. In the view of the fact that most renewable energy sources (RES), such as photovoltaic (PV), fuel cell (FC) and variable speed wind power systems, generate either DC or variable frequency/voltage AC power, a power-electronics interface is an indispensable element for the grid integration [1, 2]. In addition, modern electronic loads such as computers, plug-in hybrid electric vehicles and even traditional AC loads such as induction motors, when driven by a variable speed drive require DC power. DC micro-grids have shown advantages in terms of efficiency, cost and system that can eliminate the DC/AC or AC/DC power conversion stages required in AC micro-grids for the integration of RES and loads.

DC micro-grids like AC ones can operate in either grid-connected or islanding mode [3]. In the grid-connected mode, RES are expected to work in maximum power point tracking (MPPT) and deliver the maximum available power to the grid. The utility grid is supposed to support the balance of power and regulate the DC voltage. In the islanding mode of operation, there is no dominant source and the local energy sources are responsible for micro-grid voltage regulation and load variation. Owing to the intermittent nature of RES and variation in the load demand, energy storages (ES) are requisite for the consistent operation of the renewable systems and DC

voltage regulation. The load and the RES power generation profiles are the two most important factors for determining the kind of ES. Several technologies for ES are available, among which batteries have been used extensively in micro-grid applications [4–6]. Considering the cost of the battery, adopting a proper charge/discharge control strategy for the efficient use of the battery in order to achieve high state-of-charge (SoC) and prolonging its life is a serious issue. In the charging mode, a battery charger is necessary to ensure a full SoC of the battery and prevent overcharging, as well as increasing the battery lifetime. It is shown in [7] that the efficient charging is fulfilled in three stages: constant current, constant voltage and floating charge stages. In addition, according to the operation modes of micro-grids, during the charging process the controller may be required to regulate the DC voltage by controlling the battery rate of charge. In discharging mode, the control system is supposed to limit the battery current and avoid over-discharging throughout the time that battery regulates the DC voltage by the control of energy discharge. As a result, a suitable power management scheme is needed in order to properly recognise the micro-grid operating mode and coordinate the sources, storages and loads to obtain the micro-grid necessities in different operating modes while considering battery limitations and features. Two main approaches, that is, active and distributed control strategies have been followed in the literatures and appropriate controllers are implemented. In active methods [7–11], the structure is based on the direct coupling of different energy sources to the common DC bus, and the power

management is done by a central power control unit via real-time detection of generated power and load demand. These power management schemes are accepted for their better stability, accuracy and fast response, however, in a DC micro-grid, sources and storage systems are dispersed throughout the grid where active power management schemes require a reliable and fast communication link, which is not technically accepted in micro-grids mainly due to reliability issues. Distributed power management schemes [5, 6, 12–14] have shown to be more reliable for micro-grid management and can be implemented devoid of a communication link. These approaches utilise DC voltage level changes to realise the communications between various sources/storages in the micro-grid [14]. However, unlike the active method, this control strategy cannot be applied directly for ES, because DC micro-grid consists of different operating modes in which the battery has dissimilar functionality with somewhat conflicting dynamic and steady-state characteristics. These modes include charging in grid-connected mode and charging/discharging in islanding mode. According to the characteristic of micro-grid, researchers have indicated the need for different sets of controllers for charge/discharge control in different operating modes. Xu and Chen [5] propose strategies for distributed coordination and control of sources, loads and ES in a DC micro-grid. A battery management system based on SoC estimation is designed for battery controller, which switches to the proper control loop in order to provide necessary DC voltage regulation under different conditions. A distributed control strategy for the control of battery in a modular PV system is proposed in [6]. Appropriate control loops are developed for different operation modes in which the DC voltage determines the control mode for the sources and the storages in the micro-grid. Power flow control of batteries is discussed in [13] for the desired performance of batteries in micro-grid applications. Fuzzy switching controller is used to recognise the micro-grid operation mode and activate the proper control set for charge/discharge of the battery.

The main issue associated with the aforementioned distributed control strategies is that the performance of the micro-grid is deeply dependent on the ability of the power management strategy to accurately and quickly detect the micro-grid operating mode, particularly in transients, disturbance and in transition from one operating condition to the other which may cause multiple erroneous switching between the control sets. Besides, these switching control strategies need careful control design in order to prevent any instability [15, 16]. This problem is more serious in cases where a time-delay exists in the detection of switching situation [17]. The other issue that is important to be considered for the effective utilisation of the battery is the power limitation of battery and upper/lower limits of SoC, which is not fully considered in these studies.

In order to avoid or eliminate the abovementioned shortcomings, this paper proposes a unified distributed charge/discharge control strategy for the distributed integration of BESS in DC micro-grids. The proposed method adapts BESS to employ the same control architecture for islanding mode as that arranged for the grid-connected operation with no need to have the knowledge of the micro-grid operating condition or recognising the moment of islanding, which does not require forced switching between the sets of controllers and provides smooth transfer between the micro-grid operating modes. In addition, it assumes the same power converter

circuit, current-mode control structure and mechanism that are generally used in commercial battery chargers [11]. The proposed control strategy includes the coordination between the BESS and RES, which enables stable operation of the micro-grid during different operating modes, that is, grid connected, islanded or transition between these two modes, while considering load shedding, battery SoC and battery power limitation. Extending the concepts proposed in [18, 19] for the effective battery charging, this paper presents a controller for charging the battery in normal grid-connected operation mode that considers battery characteristics and limitations. Then, the controller is augmented with an outer grid voltage control loop in order to perform the DC voltage regulation in islanding operation by means of the battery charge/discharge control. This control loop determines the battery reference voltage by sensing the local grid voltage. The idea is to properly control the battery voltage in order to manage the battery power (charging/discharging rate). However, in normal grid-connected mode, this grid voltage control loop is saturated and the battery charging algorithm takes over to permit possible charging of the battery. The paper is organised as follows. In Section 2, the proposed control scheme for battery charge/discharge is discussed. Small signal modelling of the BESS and the controller design are presented in Section 3. The DC micro-grid modelling and the power management strategy for different cases are described in Section 4. SIMULINK/MATLAB simulations and laboratory experimental tests validate the effectiveness of the proposed system and control strategies, and the results are shown in Sections 5 and 6. Finally, the main conclusions are given in Section 7.

2 Proposed BESS control scheme

In order to afford operation of the micro-grid in both grid-connected and islanding states, the battery control system should be able to regulate the DC bus voltage and provide a stable grid operation. The primary source of power generation for the studied DC micro-grid is considered to be of renewable ones, which are often controlled to operate at MPPT while the battery meets the sensitive load demand to maintain a continuous supply of power in case of fluctuations in the main grid or during islanding operation. Different operating modes are considered for the DC micro-grid, which are summarised in Table 1. In mode I, the DC micro-grid is connected to the main grid, the RES is working in MPPT, BESS in charging or floating state, while the DC bus voltage and power balance are controlled by the grid-side voltage-source converter (GS-VSC). Modes II and III correspond to the islanding state of the micro-grid where the RES is operating in MPPT and the insufficient/surplus power is balanced by discharging/charging of the BESS. In these two modes, the BESS is responsible for voltage regulation. In mode IV, the micro-grid is also in islanding state and the required power is larger than the total maximum power of RES and BESS, or the battery is in a low SoC. Consequently, in order to maintain the system stability load shedding is required [3].

2.1 Battery modelling

A proper charge–voltage model is essential in order to study the battery behaviour during charge and discharge conditions. Owing to the non-linear characteristic of battery,

Table 1 DC micro-grid operating modes

Mode	Micro-grid state	PV state	BESS state	GS-VSC
I	grid-connected	MPPT	charging/off	inverting/rectifying mode
II	islanding	MPPT	discharging/off	disconnected
III	islanding	MPPT	charging/off	disconnected
IV	islanding	MPPT	limited	disconnected

its proper representation in the controller is a challenge. In a renewable-based micro-grid with an intermittent power generation profile, it is imperative to consider the dynamical behaviour of batteries. Different models for simulating battery behaviour with different degrees of complexity and precision are available. These models can be categorised into three groups; electrochemical, mathematical and electrical models. Electrochemical models [19] characterise the battery mechanisms by a set of differential equations. Such models are too complex for real-time control purposes and are useful for evaluating actual conditions of the battery. In mathematical models [20], the performance of the battery is simply described by some empirical equations with no particular practical meaning. Electrical models [7, 21, 22] represent the battery behaviour with basic electrical elements, such as voltage and current sources, resistors and capacitors. Although this kind of model ignores some chemical reactions in the battery such as stratification, but it is more intuitive, relatively simple and adequate for investigating the control system that makes it a widely effective model for control simulation purposes [22]. Various kinds of such electrical models have been proposed in the literatures. The simplest electrical model of a battery contains an ideal voltage source in series with a constant internal resistance [23]. Another commonly used model is the Thevenin equivalent model [24], which consists of an ideal no-load battery voltage, series internal resistance in series with a parallel combination of over-voltage resistance and capacitance. In the Thevenin equivalent model, transient behaviour of the battery can be simulated. However, this model just considers battery discharging mode, and the charging and run-time behaviour of the battery cannot be simulated. Models that are more realistic have been proposed to take into account the non-linear parameters and the battery dynamical behaviour [22]. A dynamic battery model for lead-acid batteries is proposed in [25]. This electrical model characterises different working zones for battery run-time, that is, saturation, overcharge, charge, discharge and over-discharge zones shown in Fig. 1. Results show that this model can satisfactorily demonstrate the behaviour of batteries during the charge/discharge processes; however, the transient performance of battery cannot be investigated through such models [22].

According to the above discussion, for the battery modelling and in order to apply a proper model for both charging and discharging processes, a combinatory model based on the run-time based and Thevenin model is modified and used in this paper in order to simulate charge/discharge behaviour of the battery in the proposed control strategy. The equivalent circuit model is depicted in Fig. 2.

In this model, the voltage source V_g represents the battery open circuit voltage, R_{sb} models the internal resistance of the battery, which contains the effect of operating point

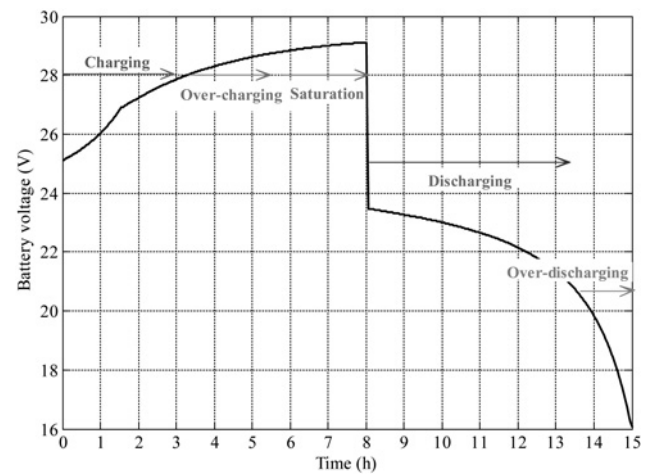


Fig. 1 Different working zones for battery run-time [26]

(I , SoC). Owing to the cost consideration, higher availability and ease of manufacturing, lead-acid battery is still widely used in different applications such as micro-grids [4, 11]. The capacity-based normalised forms of the equations for lead-acid battery are as follows [25]:

Discharge zone

$$V_g = 2.085 - 0.12(1 - \text{SoC}) \quad (1)$$

$$R_{sb} = \frac{I}{C_{10}} \left(\frac{4}{1 + I^{1.3}} + \frac{0.27}{\text{SoC}^{1.5}} + 0.02 \right) \quad (2)$$

where $\text{SoC} = (1 - (Q/C))$, $Q = It$. C_{10} is the nominal capacity (in ampere-hours) after a 10 h charging.

Charge zone

$$V_g = 2 + 0.16(\text{SoC}) \quad (3)$$

$$R_{sb} = \frac{I}{C_{10}} \left(\frac{6}{1 + I^{0.86}} + \frac{0.48}{(1 - \text{SoC})^{1.2}} + 0.036 \right) \quad (4)$$

Furthermore, the RC network (R_{tb} , C_{tb}), similar to that in Thevenin model, simulates the transient response. The parameters are [21]

$$R_{tb} = 0.086 I^{-0.67} (70.3 - 11.66 V_{oc} + 0.49 V_{oc}^2) \quad (5)$$

$$C_{tb} = (326.5 I^{-1.1} R_{tb})^{-1} \quad (6)$$

2.2 Control algorithm for the battery

According to the operating modes presented in Table 1, the battery is expected to be charged or discharged under different grid operating modes. Efficient use of the battery and its effective life highly depends on the battery charge

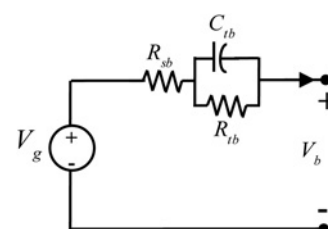


Fig. 2 Modified equivalent circuit model of the battery

and discharge method. A commonly applied charging strategy is based on on/off control [18]. However, this control method is not suitable for micro-grid applications since it causes prolonged charging process. Furthermore, in the islanding mode and during the off time, no energy is transferred to the battery. As a result, the accessible renewable energy may not be stored properly and the voltage regulation task cannot be carried out by this control strategy in case of battery charging [7]. Another proposed method for battery charging is by means of the SoC estimation [26]. However, accurate estimation of the SoC and its implementation is complicated. In [7], a battery charging strategy is developed for PV applications in which the charging process is fulfilled in three stages as shown in Fig. 3. During the first stage, the battery is charged under constant current according to the nominal battery charging current. When the battery voltage reaches the gassing voltage [25], the second stage begins and the charging is completed via constant voltage charging mode. The third stage corresponds to the floating charge where the battery is fully charged. It has been shown that this algorithm can be effectively used for battery charging in renewable energy systems [7]. This algorithm is implemented in the proposed control system for charging the battery. However, since the battery is planned to regulate the DC voltage during different operating modes, it is required to disregard this charging algorithm in the case where the micro-grid is islanded and the generated renewable energy is in excess of the demanded load. In such operating condition, the controller is designed to charge the battery in a constant voltage mode while keeping the DC bus voltage regulated in the permissible range.

Besides the charging, the discharging control of the battery is also important in order to smoothly regulate the DC voltage by the control of power discharge in accordance with the demanded load. Furthermore, the control system is designed to limit the battery discharge current and avoid over-discharging, when SoC of the battery is beneath the tolerable value, or over-loading, when the demanded power is more than battery maximum power. In such cases, a load-shedding strategy should be followed. The load shedding and power management strategies are reviewed in Section 4.2.

2.3 Proposed battery charge/discharge control scheme

A grid interface is required for the connection of battery to the DC micro-grid. One of the most flexible methods for the

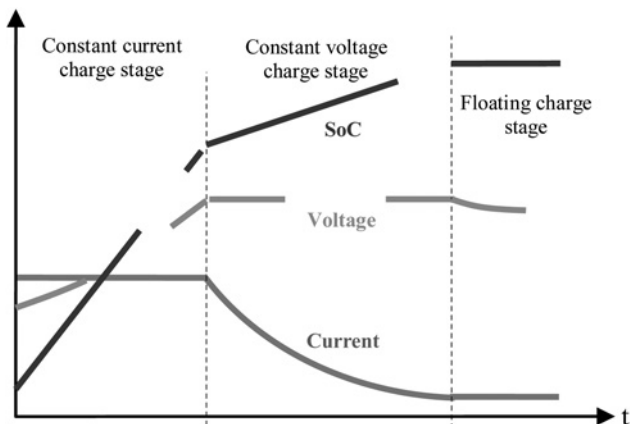


Fig. 3 Charging stages for battery

superior performance of battery is to connect it by a proper DC/DC converter [27]. A bi-directional buck-boost DC/DC converter shown in Fig. 4 is used in the current study for the battery interface. In this circuit L , R_L represents the converter input filter and C_o , R_o are the output filter. Under different micro-grid conditions, the battery operates at charging, discharging or floating modes, and the modes are managed according to the DC bus voltage condition at the point of BESS coupling.

The proposed control strategy regulates the converter input voltage (or equally the battery terminal voltage) during the charging process. This approach allows controlling the battery charge/discharge and protecting over-charge/discharge with no need to estimate the battery SoC that is usually a difficult task. In case of voltage control mode, for example, in micro-grid islanding operation, an external voltage control loop adjusts the converter reference input voltage to achieve the grid voltage regulation.

The overall block diagrams of the proposed control topologies for the BESS are shown in Fig. 5. The DC/DC boost converter employs the peak current-mode (PCM) control with slope compensation [28] to control the input voltage. The PCM control is a two-loop control system: a voltage loop with an additional inner current loop that monitors the inductor current (or equally the battery current) and compares it with its reference value (I_{bat}^{ref}) which is generated by the battery voltage controller shown in Fig. 6. The battery current limiter block limits the current to the maximum battery charging current (I_c^{max}) and discharging current (I_{dc}^{max}) values. In the proposed control strategy, a combined outer voltage loop is added to generate the converter reference voltage command (V_{bat}^{ref}) by means of considering both the battery voltage set point (V_{bat}^{sp}) and the reference grid voltage control value (V_{VC}^{ref}). Converter input voltage is regulated to control the battery SoC or the output DC voltage when needed. The grid voltage

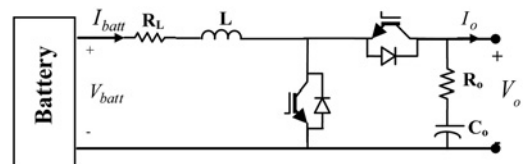


Fig. 4 Bidirectional buck-boost battery converter

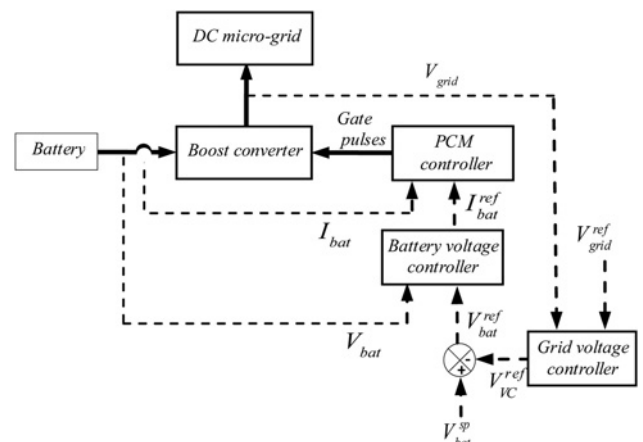


Fig. 5 Block diagram of the proposed control topologies for BESS

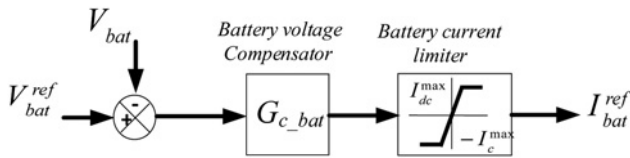


Fig. 6 Block diagram of the battery voltage controller in Fig. 5

controller, shown in Fig. 7, compares the grid voltage (V_{grid}) with the islanded grid reference voltage (\tilde{V}_{island}^{ref}). \tilde{V}_{island}^{ref} is selected to be greater than the maximum value of the controlled grid voltage by GS-VSC. Therefore, in the grid-connected mode, $V_{grid} - \tilde{V}_{island}^{ref} \leq 0$ and the generated signal will be limited to zero by the negative limiter block. In this case, the battery voltage controller loop controls the battery charging process. On the other hand, in case of islanded micro-grid operation with insufficient renewable power generation, the grid voltage control loop will go positive and shifts V_{bat}^{ref} by controlling V_{VC}^{ref} and the insufficient power will be supplied by controlling the discharge of the battery. \tilde{V}_{island}^{ref} is generated according to the battery output voltage which resembles the SoC. When the battery voltage (V_{bat}) is above the minimum acceptable battery voltage (V_{bat}^{min}), that corresponds to the secure SoC, the relay block sets the output to V_{grid}^{ref} . On the other hand, if $V_{bat} < V_{bat}^{min}$ the battery is in low SoC and there is not enough charge for supplying the total load. In this case, \tilde{V}_{island}^{ref} is set to the shedding voltage (V_{shed}) in order to trigger the load-shedding system. Accordingly, some unimportant loads in the micro-grid will be shed and energy for sensitive ones will be saved. An anti-windup control is also added to compensate the saturation of the control variable, which is commonly caused in a controller implementation and results in integral windup. The combination of these two voltage control loops is exploited to instantaneously balance the system power and controlling the grid voltage in required operating modes. Moreover,

when the available maximum discharge power of the battery is less than the demanded power, the load-shedding system will trip the required amount of the load to avoid over-discharge of the battery.

3 Small signal modelling and controller design

According to the battery equivalent circuit model in Fig. 2 and using the averaging method [28] for the DC/DC converter, the BESS model can be expressed by the following equations

$$\frac{di_L}{dt} = \frac{1}{L} [-(R_L + R_{sb})i_L + (1 - d)v_o - v_{tb} + v_g] \quad (7)$$

$$\frac{dv_o}{dt} = \frac{1}{C_o} [(1 - d)i_L - i_o] \quad (8)$$

$$\frac{dv_{tb}}{dt} = \frac{1}{C_{tb}} [i_L - \frac{1}{R_{tb}}v_{tb}] \quad (9)$$

and battery output voltage is

$$v_b = v_g - R_{sb}i_L - v_{tb} \quad (10)$$

The averaged small-signal state-space model of the BESS is derived by the linearisation of (7)–(9), and by taking the inductor current (\hat{i}_L), output voltage (\hat{v}_o) and the capacitor voltage in the battery model (\hat{v}_{tb}) as the state variables and duty cycle (\hat{d}) and output current (\hat{i}_o) as the inputs. The simplified small-signal block diagram model of the system is illustrated in Fig. 8. Related transfer functions are found using the state-space model and expressed in Appendix.

In Fig. 8, F_m , F_v and F_o model the peak-current mode controller with slope compensation [28]. These parameters

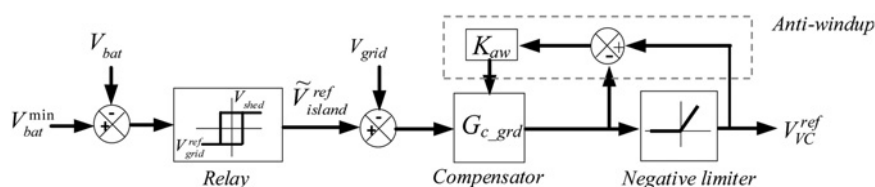


Fig. 7 Block diagram of the grid voltage controller in Fig. 5

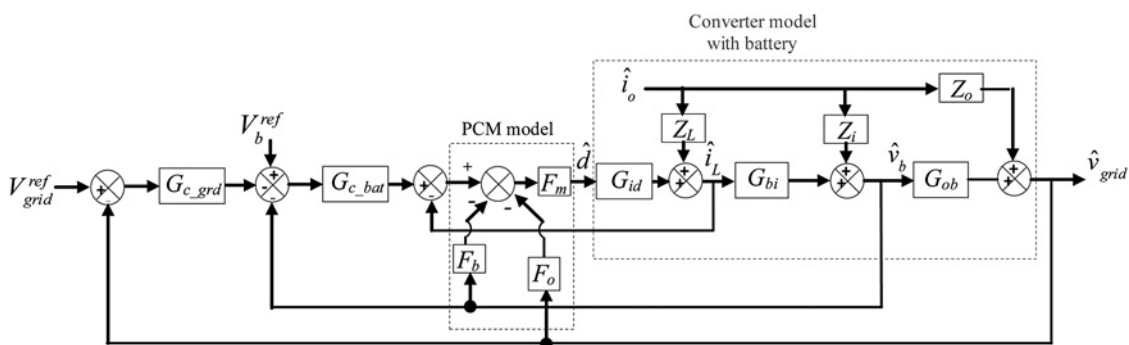


Fig. 8 Small signal block diagram model of the BESS

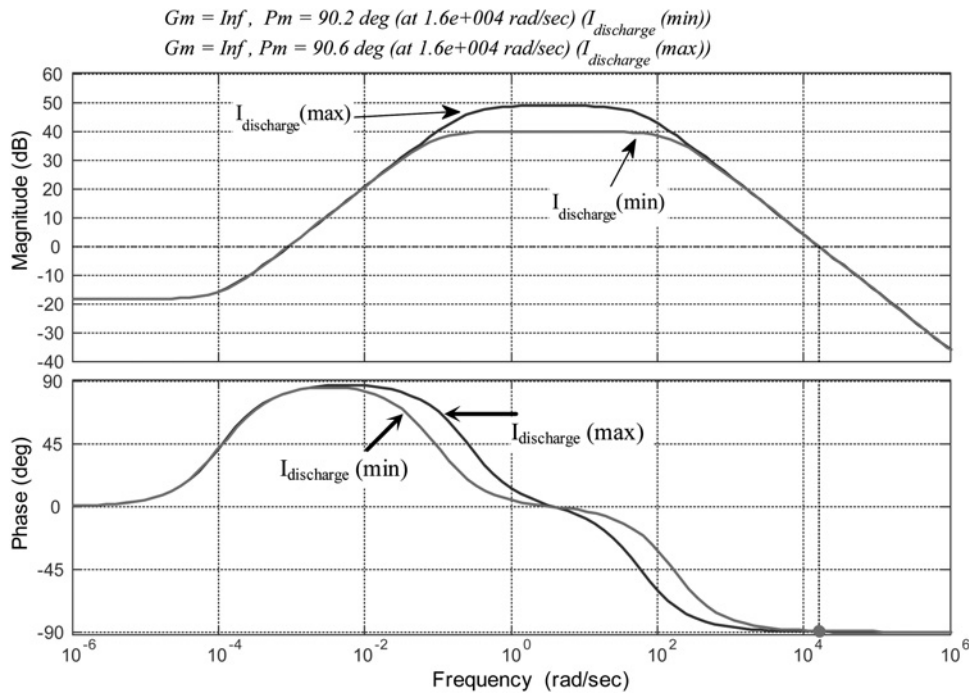


Fig. 9 Bode plot of G_{bi} under minimum and maximum discharge current conditions

are defined as follows

$$F_o = -\frac{D^2 T_s}{2L} \tag{11}$$

$$F_b = \frac{D^2 T_s}{2L} \tag{12}$$

$$F_m = \frac{1}{M_a T_s} \tag{13}$$

where T_s is the period of gate-pulses and M_a is the slope of the artificial ramp for the slope compensation.

Since the model parameters depend on the state of charge and the battery current, it is required to analyse the model for the worst operating condition in designing the battery controller. The important role of the BESS is in discharging mode for regulating the grid voltage during occurrence of different disturbances. Bode plots for the system transfer functions G_{id} and G_{bi} that depend on the battery model are plotted in Figs. 9 and 10 for minimum and maximum charging current conditions based on the parameters shown in Table 2 for a lead-acid battery. According to these figures, the stability margin in these two conditions is not different significantly. However, the maximum charge current condition has a lower bandwidth. Therefore the control system is designed for the maximum discharge current and simulated for other operating points to verify the controller performance.

4 Operation and modelling of DC micro-grid

4.1 Renewable-energy-based DC micro-grid characteristics

The previous section dealt with the modelling and control of BESS. In order to evaluate the performance of the storage system in a renewable-energy-based DC micro-grid, a

simple micro-grid schematically shown in Fig. 11 is selected as the study case. The micro-grid contains PV system as a renewable energy along with the BESS described in previous sections. The micro-grid is also connected to the main grid via a VSC. The function of GS-VSC is to regulate the DC-link voltage during grid-connected mode. A two-level VSC is used to link DC and AC grids. Current-mode control approach [29] is exploited for real/reactive power control at AC side. Thus, the amplitude and the phase angle of the VSC terminal voltage are controlled in a dq rotating reference frame. The DC-link voltage control is achieved through the control of real power component. DC voltage dynamics can be formulated based on the principle of power balance, as

$$\frac{d}{dt} \left(\frac{1}{2} C \times V_{DC}^2 \right) = P_{dc} - P_{ac} \tag{14}$$

$$P_{dc} = V_{DC} \times i_{grid}^{DC} \tag{15}$$

A DC/DC converter is also used for the connection of PV arrays to the micro-grid. A general perturbation-and-observe MPPT method along with the control system in [11] is implemented for the PV system in the current study.

Composite DC loads including constant power and constant impedance terms are modelled to verify the stable operation of the system for different micro-grid operating modes.

4.2 Power management strategy

In a real grid, there may be multiple of sources dispersed throughout the grid, thus a distributed power management strategy is needed to coordinate the sources/storages effectively. The modified DC-bus signalling method [3] is used in this paper to coordinate the proposed battery controller with the PV generation system and to obtain the

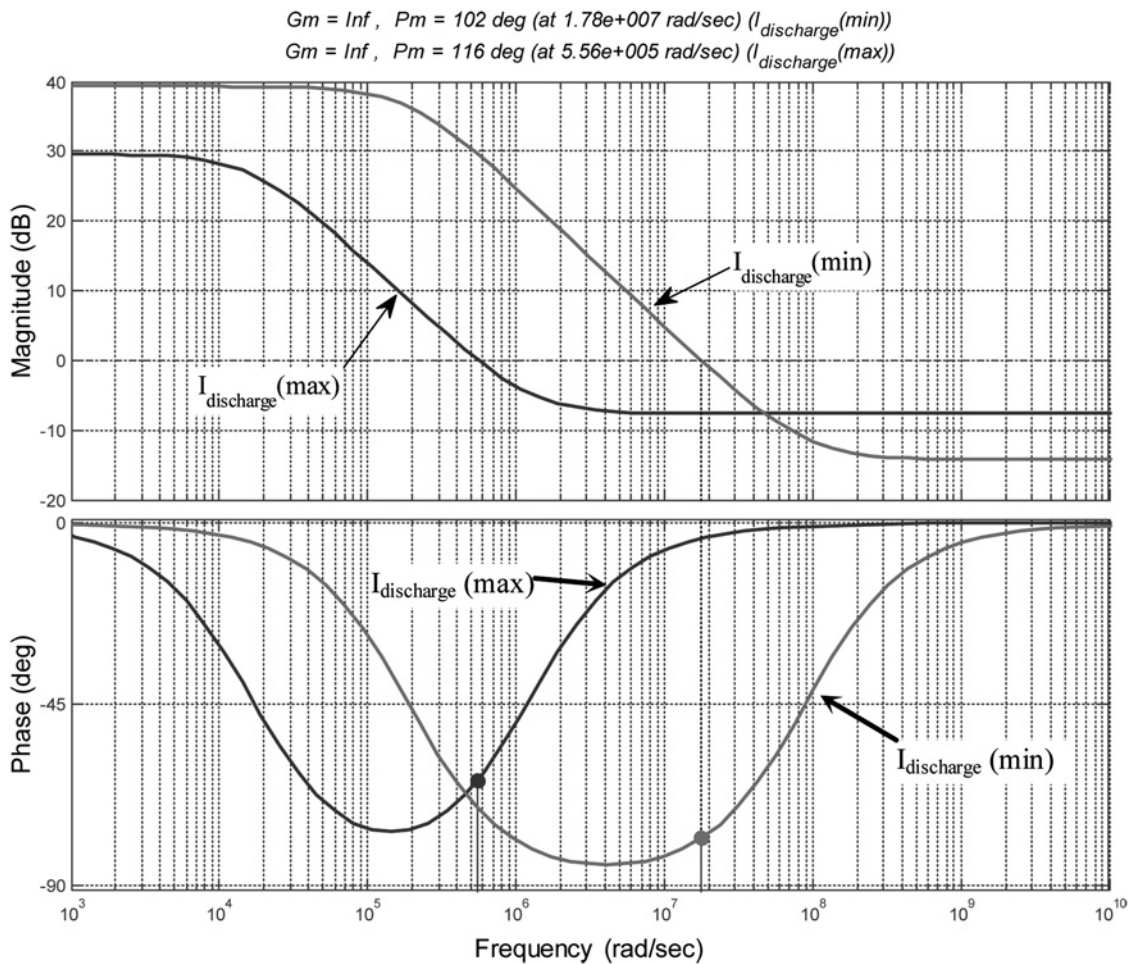


Fig. 10 Bode plot of G_{bi} under minimum and maximum discharge current conditions

Table 2 BESS rating

BESS	
type	lead-acid
rating	300 V, 120 Ah
battery converter	5 KHz
L, R_L, C_o, R_o	15 mH, 0.02 Ω , 1 mF, 0.025 Ω

power balance and stable operation of DC micro-grid under various generation or load conditions. In this approach, DC-bus voltage level change is utilised to communicate between sources and storages and to recognise different operating modes according to the voltage levels defined in Table 3. The voltage thresholds are set as follows:

- $V_{\text{VSC}} = 1.05$ pu reference voltage for the GS-VSC;
- $V_{\text{ref}}^{\text{bat}} = 0.95$ pu reference voltage for BESS.

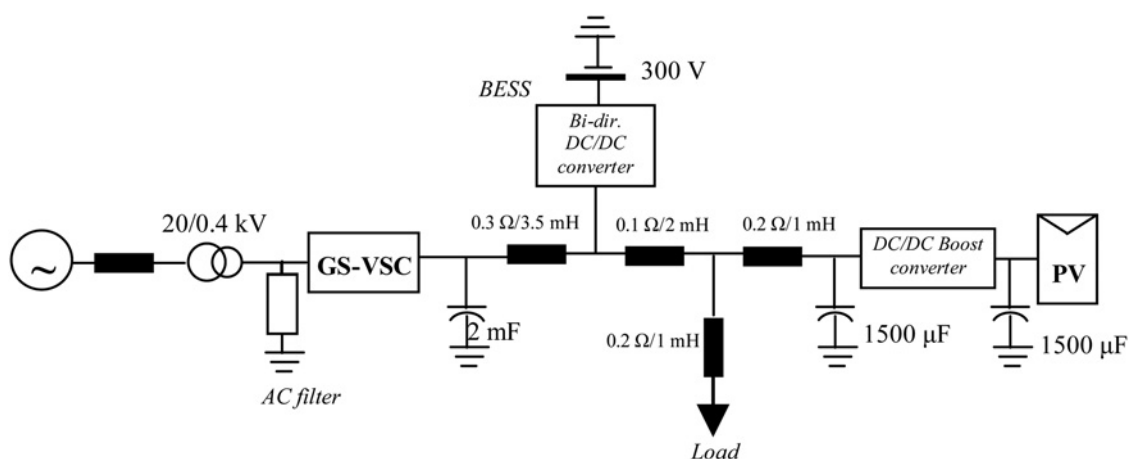


Fig. 11 Schematic diagram of the simulated DC micro-grid

Table 3 Voltage levels for recognising different operating modes

Operating mode	DC-link voltage
mode I, III	$V_{dc} < V_{ref}^{bat}$
mode II	$V_{dc} < V_{ref}^{bat}$
mode IV	$V_{dc} \leq V_{shed}$

As discussed earlier, a load-shedding scheme may also be necessary to protect the system against instability when the demanded power exceeds the maximum deliverable power. In this case, DC voltage cannot be fully controlled and will continue decreasing from the minimum allowable value. In order to prevent the total collapse of the DC micro-grid, a prioritised load shedding is implemented based on the local DC voltage measurement without the need for communication. MDBS is applied here based on the IEC standard inverse definite minimum time curve for implementing the load shedding [3]. The voltage thresholds to start load shedding is set as $V_{shed} = 0.9$ pu.

5 Case studies and simulation results

In order to validate the proposed control method for distributed control of battery ES in renewable-energy-based DC micro-grids, system simulations have been carried out using SIMULINK/MATLAB. A schematic diagram of the studied DC micro-grid is shown in Fig. 11. Detailed ratings of the system elements are presented in [3]. The following considerations are regarded for a stable operation of the system:

- Considering the non-deterministic characteristic of PV power generation and in order to ensure supply of DC load demand, the power rating of the GS-VSC is selected as the sum of maximum DC grid load demand and maximum charging power of batteries.
- The sum of maximum discharging power of batteries should be greater than the power of sensitive loads in the DC grid.
- The average power of PV array is also assumed to be equal to the sum of DC load power demand and battery charging power.

Based on the battery model and using the small-signal model of the system, the compensator is designed as (16) for the grid voltage control loop.

$$G_{c_grd} = 2 \times 10^5 \left(\frac{s + 20}{s(s + 10^5)} \right) \quad (16)$$

The same procedure is done for the inner loop compensator and a proportional-integral controller is designed as the following equation

$$G_{c_bat} = 1 + \frac{0.01}{s} \quad (17)$$

Regarding the abovementioned conditions, different operating scenarios are simulated and the control methods to obtain a stable DC micro-grid are tested. The system is simulated for the two states of micro-grid, that is, grid connected and islanding and considers different operating modes and possible transition between these modes.

Different operating scenarios are simulated in order to validate the performance of the BESS in controlling the DC voltage and supplying the load in the micro-grid. The scenarios and study cases are described in the following sections.

5.1 Case 1

The battery charging process is simulated in this case. For this purpose, the DC micro-grid is supposed to be connected to an external AC micro-grid, a portion of the demanded load is supplied by the PV and the insufficient power plus the battery charging power is provided by the GS-VSC by means of rectifying the AC power. The GS-VSC is also responsible for DC voltage regulation. Battery SoC is selected to be 85% in which the battery voltage is near the upper limit. At first, the battery is charged in constant current mode for about 50 min. Once the battery voltage reaches the upper limit, the charger controls the charging in constant voltage mode to fulfil the battery charge. Fig. 12 shows the battery voltage, charging current and SoC during the simulation.

5.2 Case 2

This case simulates the transition from mode I to mode II. This is related to the situation where the DC micro-grid moves into the islanding mode and isolates from the main AC grid at 1 s. It is supposed that PV power generation is less than the demanded load and the insufficient power is supplied by the GS-VSC before islanding. In this case, the BESS controls the DC voltage by discharging the battery energy. Effect of load and solar insolation variation are also considered in the simulation. For example, at 4.5 s, load increases and the battery delivers more power to the DC grid and regulates the voltage as well. Operation events during this case are explained in Table 4. Simulation results

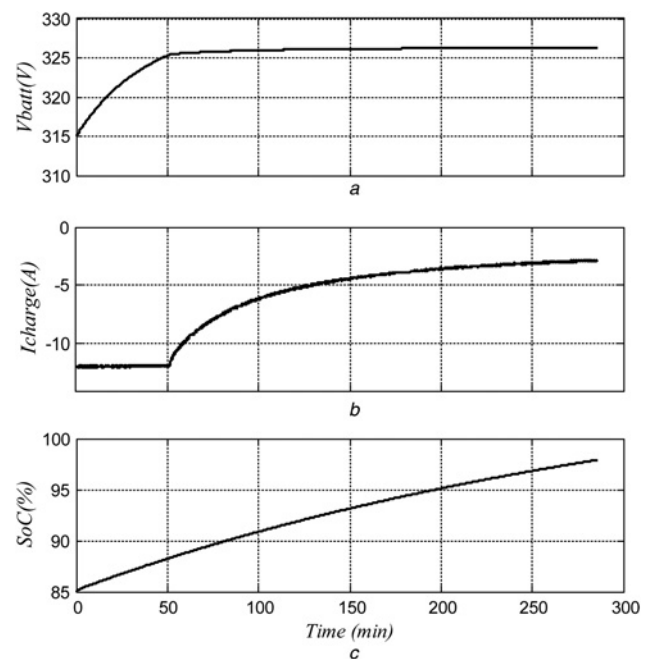


Fig. 12 Battery charging process in grid-connected mode (Case 1)

- a Battery voltage (V)
- b Battery charging current (A)
- c Battery SoC

Table 4 Operation events during case 2

Time, s	Operation event
1	transition to islanding mode
3	insolation reduces from 1000 to 800 W/m ²
4.5	10% of initial load is switched on
6	insolation increases from 800 to 900 W/m ²
7.5	10% of total load is switched off
8	insolation increases from 900 to 1000 W/m ²
9.5	10% of initial load is switched off

are shown in Fig. 13. Load, GS-VSC, PV and battery power along with DC voltage at the load point are illustrated in Figs. 13a–e, respectively. It can be deduced that the BESS can control the DC voltage in islanding transition and smoothly regulate the voltage in case of load and solar insolation variations while the PV tracks the MPP during the simulation.

5.3 Case 3

This case is similar to case 2 but it is supposed that PV power is larger than the demanded load and the battery is not fully charged, so a transition from mode I to mode III is simulated. In this case, the battery is partially charged in

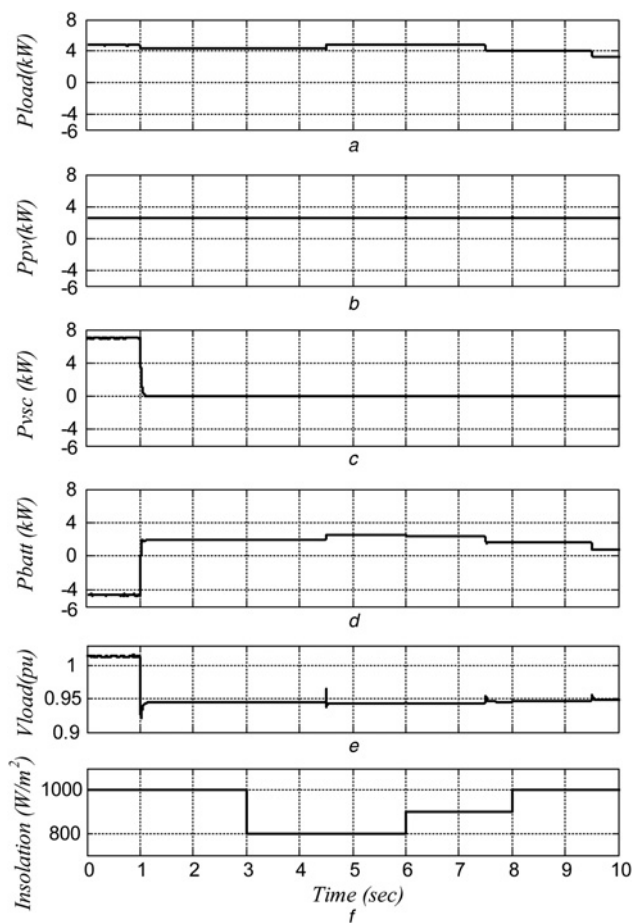


Fig. 13 System operation in transition to islanding (Case 2)

- a Total load (kW)
- b PV power generation (kW)
- c Power of the GS-VSC (kW)
- d Battery charging/discharging power (kW)
- e DC voltage at load point
- f Solar insolation variation (W/m²)

constant voltage mode and the BESS controls the DC voltage. Load, GS-VSC, PV, battery power and DC voltage at load point are illustrated in Figs. 14a–e, respectively. The effect of load and solar insolation variation on DC voltage, battery power and PV power is also considered in the simulation. Operation events during this case are explained in Table 5. It can be realised that the BESS can control the DC voltage in islanding transition and smoothly regulate the voltage in case of load and solar insolation variations while the PV tracks the MPP during the simulation.

5.4 Case 4

In this case, the load demand is greater than the total battery and PV power generation. The micro-grid is operating in mode I before islanding. At $t = 1$ s, the micro-grid moves to islanding mode and since the generated power is less than the demanded load a voltage drop is caused in the DC grid which may cause instability because of the constant power loads that exist in the grid. It should be mentioned that because of the constant impedance loads in the micro-grid, the total demanded power gets a slight decrease (about 420 W in the case study) when the voltage drops due to islanding. In order to operate the micro-grid stably, it

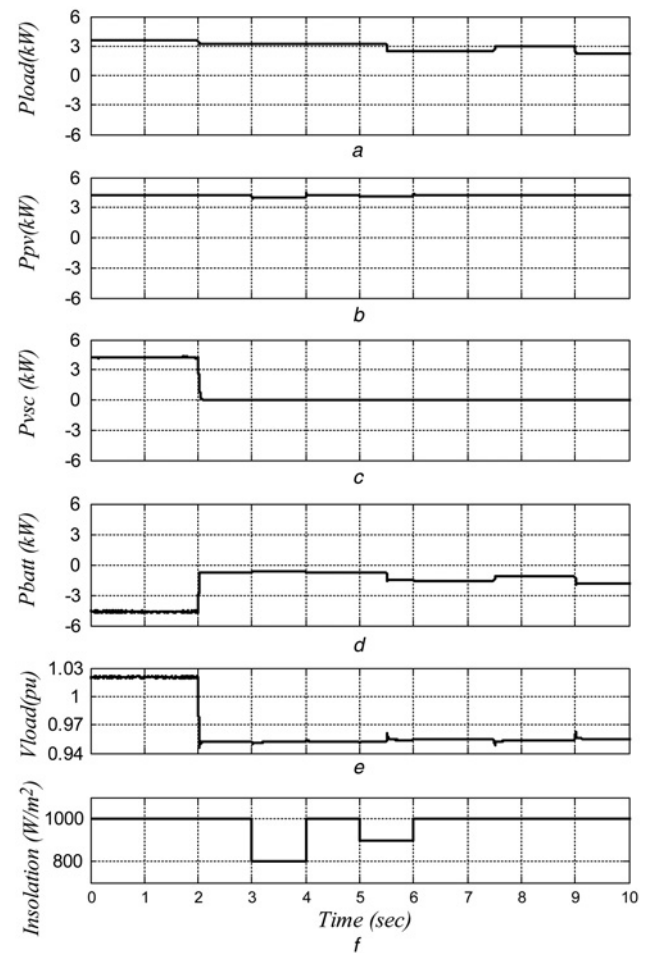


Fig. 14 System operation in transition to islanding (Case 3)

- a Total load (kW)
- b PV power generation (kW)
- c Power of the GS-VSC (kW)
- d Battery charging/discharging power (kW)
- e DC voltage at load point
- f Solar insolation variation (W/m²)

Table 5 Operation events during case 3

Time, s	Operation event
2	transition to islanding mode
3	insolation reduces from 1000 to 800 W/m ²
4	insolation increases from 800 to 1000 W/m ²
5	insolation reduces from 1000 to 900 W/m ²
5.5	30% of initial load is switched off
6	insolation increases from 900 to 1000 W/m ²
7.5	10% of initial load is switched on
9	20% of initial load is switched off

Table 6 Operation events during case 4

Time, s	Operation event
1	transition to islanding mode
1.2	a portion of load is shed in the first stage
1.4	a portion of load is shed in the second stage

is necessary to match generation and the load demand; so, the load-shedding procedure is activated and switches off the less sensitive loads. At the first step, a portion of load equal to 400 W is shut down at 1.2 s and DC voltage increases but the voltage is still below the allowable range and the second load-shedding step shuts down 800 W once more at 1.4 s and the DC voltage recovers to the standard range. Operation events during this case are explained in Table 6. Simulation results are shown in Fig. 15.

5.5 Case 5

This is similar to case 3 where the remained battery capacity is less than 50% of the nominal capacity. Under this condition, in order to preserve enough energy for supplying the critical loads, the setting for the output voltage regulation is reduced to 0.9 pu for shedding the non-important loads in the system. Operation events during this case are explained in Table 7. Simulation results are shown in Fig. 16.

6 Experimental validation

In order to validate the simulation results, the proposed control system is implemented on a small scale laboratory test system. The test system is shown in Fig. 17. The test bench consists of a 6 V/4.5 Ah lead-acid battery along with a bidirectional DC/DC converter, a PV generation unit comprising an emulated PV panel and a boost DC/DC converter, where the DC loads are connected to a 9 V DC system. A 9 V DC voltage source is used to regulate the DC bus in grid-connected mode of operation. The battery maximum charging and discharging current are 0.9 and 4.5 A, respectively and the maximum charging voltage is 6.5 V. The emulated PV panel composed of a 6 V DC voltage source connected in series with a 2.2 Ω resistor [6]. At the MPPT, the maximum output power of the PV system is 20 W. Two small RL branches are also connected in series with the PV system and BESS to emulate the DC micro-grid network. The control strategy is developed using MATLAB/SIMULINK real time windows target and the interface between the controller and the DC/DC converter is provided using ADVANTECH PCI-1711 data acquisition interface card. Real-time windows target includes a set of

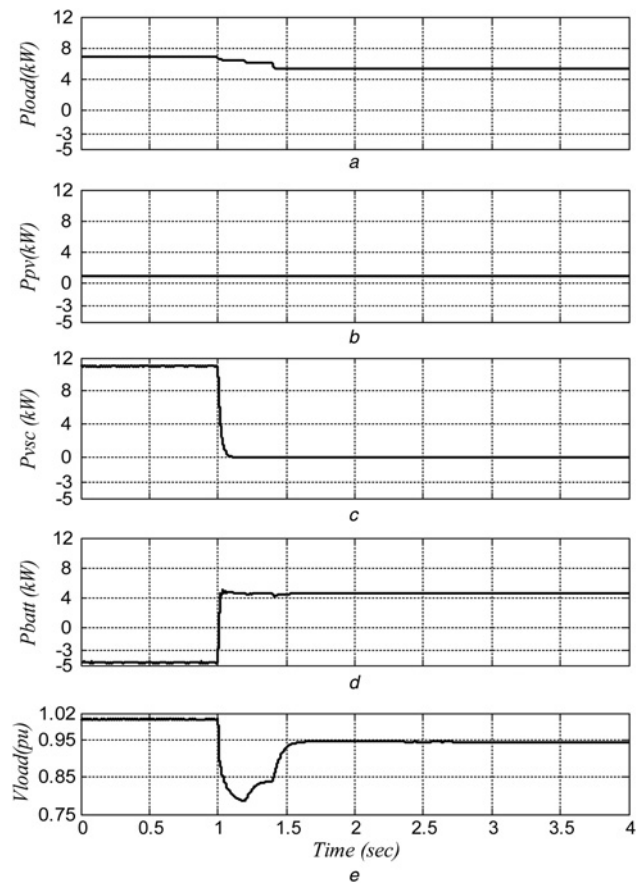


Fig. 15 System operation in transition to islanding (Case 4)

- a Total load (kW)
- b PV power generation (kW)
- c Power of the GS-VSC (kW)
- d Battery charging/discharging power (kW)
- e DC voltage at load point

Table 7 Operation events during case 4

Time, s	Operation event
1	transition to islanding mode and the voltage regulates on load-shed limit
1.5	a large portion of load is shed

I/O blocks that provide connections between the physical I/O board and the real-time model that provides hardware-in-the-loop simulations to test the real-world behaviour of the controller.

Experimental results during the transition from mode I (grid-connected) to mode II (islanding) are illustrated in Fig. 18. In Fig. 18 and other experimental results, V_{grid} is the DC grid voltage, I_{bat} is the battery current and I_{PV} is the output current of PV converter. As shown in Fig. 18, before the grid disconnection, the DC voltage is regulated by the voltage source at 9 V and the battery is charging. After the system transition to islanding, the DC voltage decreases because the local load power is greater than the PV power. Therefore the battery starts discharging to regulate the DC voltage at about 8.5 V (0.95 pu). As can be seen, the dynamic response of the controller is fast enough and only a small fluctuation occurs on the DC voltage during transition to islanding.

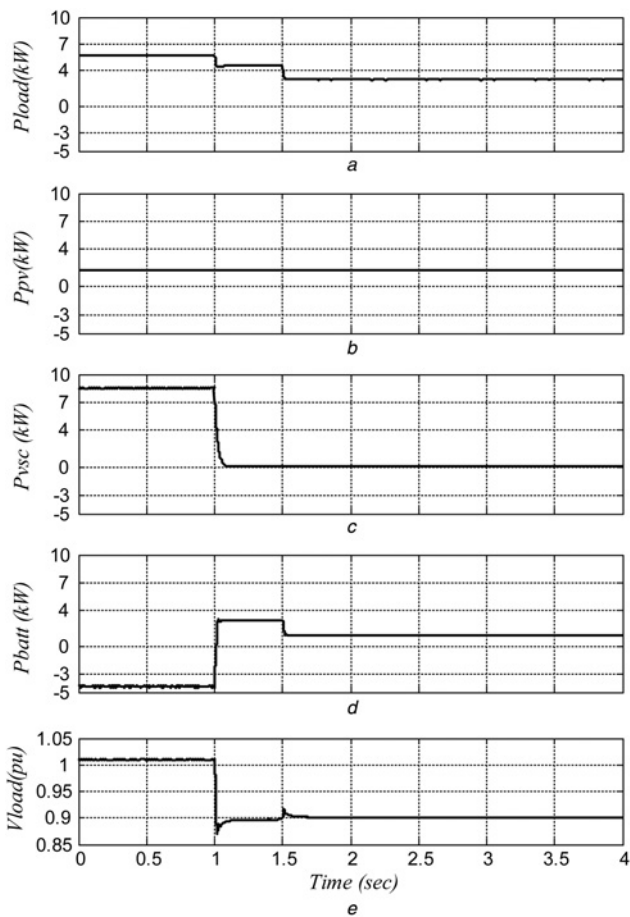


Fig. 16 System operation in transition to islanding (Case 5)
 a Total load (kW)
 b PV power generation (kW)
 c Power of the GS-VSC (kW)
 d Battery charging/discharging power (kW)
 e DC voltage at load point

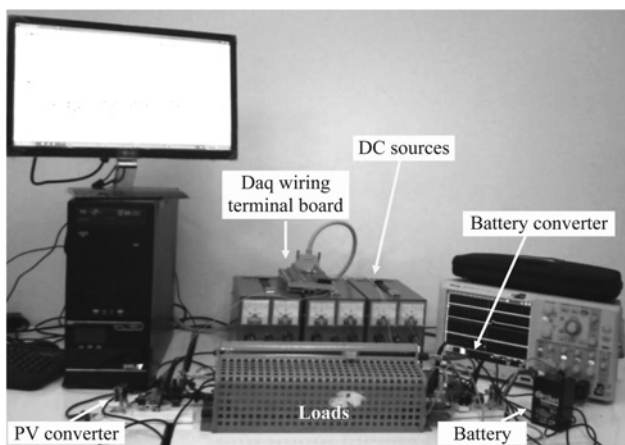


Fig. 17 Experimental laboratory test system

Experimental results during load changes in the islanding operation are shown in Figs. 19–21. Fig. 19 illustrates the case in which the load increases and the DC voltage is regulated by increasing the battery discharging current. Fig. 20 shows the same case for load decrease and the corresponding BESS response. The other test case is the condition, which the load decreases, and the load power is

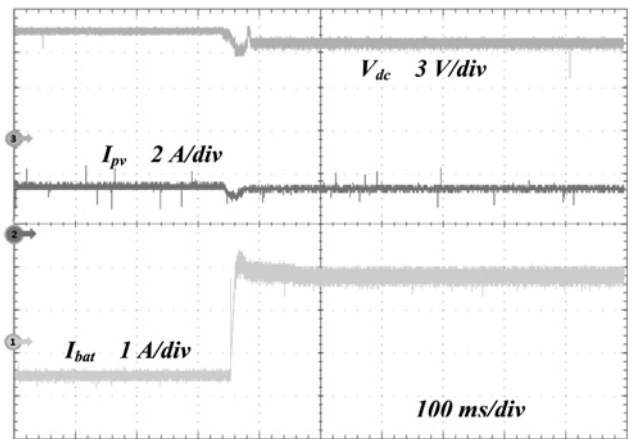


Fig. 18 Experimental results in the transition from grid-connected to islanding mode

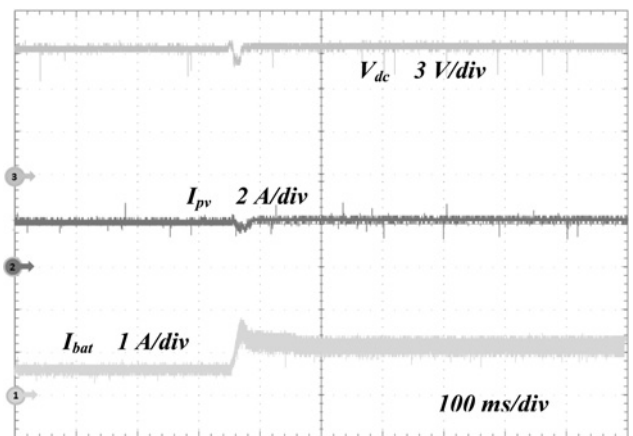


Fig. 19 Experimental results during load increase in the islanding operation

less than the PV power. In this case as shown in Fig. 21, the BESS regulates the voltage by charging the battery and absorbing the excess power. As can be seen, regardless whether the local load increases or decreases the DC

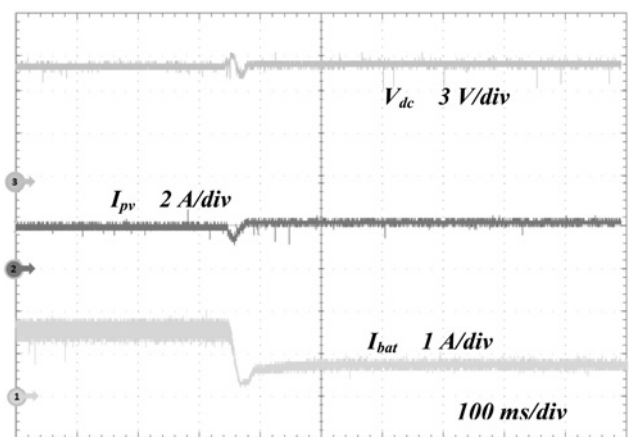


Fig. 20 Experimental results during load decrease in the islanding operation

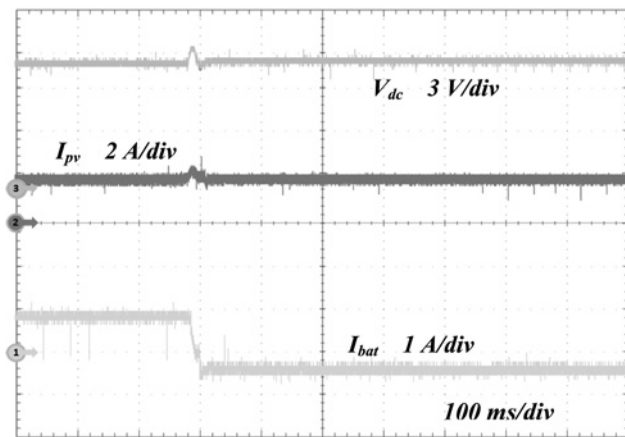


Fig. 21 Experimental results during load decrease in the islanding operation where the PV power excess the local load power

voltage has been controlled by the BESS at the reference voltage with small fluctuations.

7 Conclusion

This paper proposes charge/discharge control strategies for distributed integration of BESS in a DC micro-grid, including non-deterministic renewable sources and variable loads. The requirement of maintaining constant DC voltage is realised, considering different operating modes in grid-connected and islanded operating states. The proposed control strategy adapts BESS control system for grid-connected mode as well as the islanded operation using the same control architecture with no need to have the knowledge of the micro-grid operating mode or to switch between the corresponding control architectures which results in a smooth transfer between the micro-grid operating modes. Furthermore, the control system provides effective charging of the battery in the micro-grid. In order to achieve the system operation under islanding conditions, a coordinated strategy for the BESS, RES and load management, including load shedding and considering battery SoC and battery power limitation, is proposed. DC voltage levels are used as a communication link in order to coordinate the sources and storages in the system and acts as a control input for the operating mode adaptation during different operating conditions. System simulations and experimental tests have been carried out in order to validate the proposed control method. Results show the satisfactory DC voltage control and stable operation of the micro-grid during various disturbances and operating conditions.

8 References

- 1 Blaabjerg, F., Chen, Z., Kjaer, S.B.: 'Power electronics as efficient interface in dispersed power generation systems', *IEEE Trans. Power Electron.*, 2004, **19**, (5), pp. 1184–1194
- 2 Chiang, H.C., Ma, T.T., Cheng, Y.H., Chang, J.M., Chang, W.N.: 'Design and implementation of a hybrid regenerative power system combining grid-tie and uninterruptible power supply functions', *IET Renew. Power Gener.*, 2010, **4**, (1), pp. 85–99
- 3 Eghtedarpour, N., Farjah, E.: 'Control Strategy for distributed integration of photovoltaic and energy storage systems in DC micro-grids', *J. Renew. Energy*, 2012, **45**, pp. 96–110
- 4 Jenkins, D.P., Fletcher, J., Kane, D.: 'Lifetime prediction and sizing of lead-acid batteries for microgeneration storage applications', *IET Renew. Power Gener.*, 2008, **2**, (3), pp. 191–200

- 5 Xu, L., Chen, D.: 'Control and operation of a DC microgrid with variable generation and energy storage', *IEEE Trans. Power Deliv.*, 2012, **27**, (1), pp. 2513–2522
- 6 Sun, K., Zhang, L., Xing, Y., Guerrero, J.M.: 'A distributed control strategy based on dc bus signaling for modular photovoltaic generation systems with battery energy storage', *IEEE Trans. Power Electron.*, 2011, **26**, (10), pp. 3032–3045
- 7 Koutroulis, E., Kalaitzakis, K.: 'Novel battery charging regulation system for photovoltaic applications', *IEE Proc. Electr. Power Appl.*, 2004, **151**, (2), pp. 191–197
- 8 Hajizadeh, A., Golkar, M.A.A.: 'Fuzzy neural control of a hybrid fuel cell/battery distributed power generation system', *IET Renew. Power Gener.*, 2009, **3**, (4), pp. 402–414
- 9 Chiang, S.J., Shieh, H.J., Chen, M.C.: 'Modeling and control of PV charger system with SEPIC converter', *IEEE Trans. Ind. Electron.*, 2009, **56**, (11), pp. 4344–4353
- 10 Jiang, W., Fahimi, B.: 'Active current sharing and source management in fuel cell–battery hybrid power system', *IEEE Trans. Ind. Electron.*, 2010, **57**, (2), pp. 752–761
- 11 Fakhm, H., Lu, D., Francois, B.: 'Power control design of a battery charger in a hybrid active PV generator for load-following applications', *IEEE Trans. Ind. Electron.*, 2011, **58**, (1), pp. 85–94
- 12 Zamora, R., Srivastava, A.K.: 'Controls for micro-grids with storage: review, challenges, and research needs', *Renew. Sustain. Energy Rev.*, 2010, **14**, pp. 2009–2018
- 13 Abdollahi Sofla, M., Wang, L.: 'Control of DC–DC bidirectional converters for interfacing batteries in microgrids'. IEEE PES Power Systems Conference and Exposition (PSCE), Phoenix AZ, 2011, pp. 1–6
- 14 Schonberger, J., Duke, R., Round, S.D.: 'DC-bus signalling: a distributed control strategy for a hybrid renewable nanogrid', *IEEE Trans. Ind. Electron.*, 2006, **53**, (5), pp. 1453–1460
- 15 Liberzon, D., Morse, A.S.: 'Basic problems in stability and design of switched systems', *IEEE Control Syst. Mag.*, 1999, **19**, (1), pp. 59–70
- 16 Cheng, D., Guo, L., Dan, Y., et al.: 'Stabilization of switched linear systems', *IEEE Trans. Autom. Control*, 2005, **50**, (5), pp. 661–666
- 17 Xie, G., Wang, L.: 'Stabilization of switched linear systems with time-delay in detection of switching signal', *J. Math. Anal. Appl.*, 2005, **305**, (6), pp. 277–290
- 18 Masheleni, H., Carelse, X.: 'Microcontroller-based charge controller for stand-alone photovoltaic systems', *Solar Energy*, 1997, **61**, (4), pp. 225–230
- 19 Smith, K.A., Rahn, C.D., Wang, C.-Y.: 'Model-based electrochemical estimation and constraint management for pulse operation of lithium ion batteries', *IEEE Trans. Control Syst. Technol.*, 2010, **18**, (3), pp. 654–663
- 20 Rong, P., Pedram, M.: 'An analytical model for predicting the remaining battery capacity of lithium-ion batteries'. Proc. Design, Automation, and Test in Europe Conf. and Exhibition, 2003, pp. 1148–1149
- 21 Tian, S., Hong, M., Ouyang, M.: 'An experimental study and nonlinear modeling of discharge $I-V$ behavior of valve-regulated lead-acid batteries', *IEEE Trans. Energy Convers.*, 2009, **24**, (2), pp. 452–458
- 22 Chen, M., Rincon-Mora, G.A.: 'Accurate electrical battery model capable of predicting runtime and $I-V$ performance', *IEEE Trans. Energy Convers.*, 2006, **21**, (2), pp. 504–511
- 23 Durr, M., Cruden, A., Gair, S., McDonald, J.R.: 'Dynamic model of a lead acid battery for use in a domestic fuel cell system', *J. Power Sources*, 2006, **161**, (2), pp. 1400–1411
- 24 Salameh, Z.M., Casacca, M.A., Lynch, W.A.: 'A mathematical model for lead-acid batteries', *IEEE Trans. Energy Convers.*, 1992, **7**, (1), pp. 93–98
- 25 Achaibou, N., Haddadi, M., Malek, A.: 'Lead acid batteries simulation including experimental validation', *J. Power Sources*, 2008, **185**, pp. 1484–1491
- 26 Cheng, K.W.E., Divakar, B.P., Wu, H., Ding, K., Ho, H.F.: 'Battery-management system (BMS) and SoC development for electrical vehicles', *IEEE Trans. Veh. Technol.*, 2011, **60**, (1), pp. 76–88
- 27 Jiang, W., Fahimi, B.: 'Active current sharing and source management in fuel cell–battery hybrid power system', *IEEE Trans. Ind. Electron.*, 2010, **57**, (2), pp. 752–761
- 28 Erickson, R.W.: 'Fundamental of power electronics' (Kluwer, Norwell, MA, 1997)
- 29 Yazdani, A., Iravani, R.: 'Voltage-sourced converters in power systems – modeling, control, and applications' (Wiley, 2010)

9 Appendix

The transfer functions of the small-signal model of the BESS can be expressed as follows.

9.1 Duty cycle-to-inductor current transfer function

(see the equation at the bottom of the page)

9.2 Inductor current-to-input voltage transfer function

$$G_{bi}(s) = \left. \frac{\hat{v}_b(s)}{\hat{i}_L(s)} \right|_{\hat{i}_o=0} = -R_{sb} \frac{s + ((R_{tb} + R_{sb})/(C_{tb}R_{tb}R_{sb}))}{s + (1/C_{tb}R_{tb})}$$

9.3 Input-to-output voltage transfer function

$$G_{ob}(s) = \left. \frac{\hat{v}_o(s)}{\hat{v}_b(s)} \right|_{\hat{d}=\hat{i}_o=0} = \frac{D'}{LC_o s^2 + (R_L/L)s + D^2}$$

and to consider the output current disturbance.

9.4 Open-loop output current-to-input voltage transfer function

(see the equation at the bottom of the page)

9.5 Open-loop output current-to-inductor current transfer function

(see the equation at the bottom of the page)

9.6 Open-loop output impedance (excluding the load resistance)

(see the equation at the bottom of the page)

$$G_{id}(s) = \left. \frac{\hat{i}_L(s)}{\hat{d}(s)} \right|_{\hat{i}_o=0} = \frac{G_{id0}(C_{tb}R_{tb}s + 1)(V_o^2s + D'I_L)}{s^3 + ((R_{sb} + R_L)/L) + (1/C_{tb}R_{tb})s^2 + (((R_{sb} + R_{tb} + R_L)/(C_{tb}R_{tb}L)) + (D^2/C_oL))s + D^2},$$

$$G_{id0} = \frac{1}{V_o C_{tb} R_{tb} L}$$

$$Z_i(s) = \left. \frac{\hat{v}_b(s)}{\hat{i}_o(s)} \right|_{\hat{d}=\hat{v}_b=0} = \frac{Z_{i0}(s + (R_{sb} + R_{tb})/(C_{tb}R_{tb}R_{sb}))}{s^3 + ((R_{sb} + R_L)/L) + (1/C_{tb}R_{tb})s^2 + (((R_{sb} + R_{tb} + R_L)/(C_{tb}R_{tb}L)) + ((D^2)/(C_oL)))s + D^2},$$

$$Z_{i0} = -\frac{D'R_{sb}}{C_{tb}R_{tb}L}$$

$$Z_L(s) = \left. \frac{\hat{i}_L(s)}{\hat{i}_o(s)} \right|_{\hat{d}=\hat{v}_b=0} = \frac{Z_{L0}(s + (1/C_{tb}R_{tb}))}{s^3 + ((R_{sb} + R_L)/L) + (1/C_{tb}R_{tb})s^2 + (((R_{sb} + R_{tb} + R_L)/(C_{tb}R_{tb}L)) + (D^2/C_oL))s + D^2},$$

$$Z_{L0} = \frac{D'}{C_o L}$$

$$Z_o(s) = \left. \frac{\hat{v}_o(s)}{\hat{i}_o(s)} \right|_{\hat{d}=\hat{v}_b=0} = -\frac{1}{C_o} \frac{(s^2 + ((R_{sb} + R_L)/L) + (1/C_{tb}R_{tb}))s + ((R_{sb} + R_{tb} + R_L)/(C_{tb}R_{tb}L))}{s^3 + ((R_{sb} + R_L)/L) + (1/C_{tb}R_{tb})s^2 + (((R_{sb} + R_{tb} + R_L)/(C_{tb}R_{tb}L)) + (D^2/C_oL))s + D^2}$$